Role of anisotropic Coulomb interactions in the superexchange coupling of mixed-valent Mn_3O_4

Sangmoon Yoon,[1,2,*] Sangmin Lee,[1] Subeen Pang,[1] Miyoung Kim,[1,†] and Young-Kyun Kwon[2,3,‡]
[1]*Department of Materials Science and Engineering, Seoul National University, Seoul 08826, Korea*
[2]*Department of Physics, Kyung Hee University, Seoul 02447, Korea*
[3]*Department of Information Display and Research Institute for Basic Sciences, Kyung Hee University, Seoul 02447, Korea*

(Received 20 April 2021; accepted 19 July 2021; published 29 July 2021)

We report the importance of anisotropic Coulomb interactions in DFT+U calculations of the electronic and magnetic properties of Mn_3O_4. The effects of anisotropic interactions in Mn^{2+} and Mn^{3+} are examined separately by defining two different sets of Hubbard parameters: U^{2+} and J^{2+} for Mn^{2+} and U^{3+} and J^{3+} for Mn^{3+}. The anisotropic interaction in Mn^{3+} has significant effects on the physical properties of Mn_3O_4 including local magnetic moments, canted angle, spontaneous magnetic moment, and superexchange coupling, but that in Mn^{2+} has no noticeable effect. Weak ferromagnetic interchain superexchange observed experimentally is predicted only if a sizable anisotropic interaction is considered in Mn^{3+}. By analyzing the eigenoccupations of the on-site Mn density matrix, we find that the spin channel involving Mn^{3+} $d_{x^2-y^2}$ orbitals, which governs the 90° correlation superexchange, is directly controlled by the anisotropic interactions. These findings indicate that the exchange correction J for the intraorbital Coulomb potential is critical for the first-principles description of Mn oxides containing Mn^{3+} or Mn^{4+}.

DOI: 10.1103/PhysRevB.104.035158

I. INTRODUCTION

Mixed-valent manganese oxide Mn_3O_4 has attracted a great deal of attention because it is a prototypical example that involves Jahn-Teller distortions and geometrical frustrations as well as strong electron correlations [1–3]. Mn_3O_4 exists in a spinel structure (AB_2O_4), with Mn^{2+} and Mn^{3+} occupying tetrahedral sites (A sites) and octahedral sites (B sites), respectively, as shown in Fig. 1(a). It undergoes a cubic ($Fd\bar{3}m$) to tetragonal ($I4_1/amd$) structural phase transition at $T = 1443$ K because of the Jahn-Teller ordering at the Mn^{3+} sites [4]. It also goes through a magnetic phase transition from paramagnetic to ferrimagnetic at its corresponding Curie temperature $T_C = 41$ K, adopting a noncollinear Yafet-Kittel ferrimagnetic (YK-FiM) phase with isosceles triangles, each composed of one Mn^{2+} at the A site and two Mn^{3+} at the B_1 and B_2 sites. Spins at the A sites align ferromagnetically along the b axis, whereas spins at the B_1 (B_2) point with a canted angle of θ_c toward the $+c$ axis ($-c$ axis) from the $-b$ axis as shown in Fig. 1(b) [5,6]. Additionally, the magnetic structure of Mn_3O_4 strongly couples to its orbital, charge, and lattice, which leads to novel magnetodielectric [7,8], magnetoelastic [2,3,9,10], and magnetocaloric [11] responses at low temperatures. The exchange couplings of Mn_3O_4 have been quantitatively estimated from the spin-wave excitations measured by inelastic neutron experiments, and the results revealed that the exchange interactions are determined by the direct orbital overlap and 90° superexchange coupling between two Mn^{3+} via an oxygen bridge [10,12]. Meanwhile, Mn_3O_4 always exhibits an insulating behavior with a band gap of about 2.0 eV [13–15].

Mn_3O_4 is a challenging system to examine using first-principles calculations because strong electron correlations are combined with multiple degrees of freedom such as spin, orbital, charge, and lattice. Nevertheless, Mn_3O_4 has been investigated extensively using several computational methods over the last several decades [16–19]. Charter *et al.* used Hartree-Fock calculations to estimate the band structure, magnetic ground state, and exchange coupling constants of Mn_3O_4 [16]. Although the Hartree-Fock method reproduced an insulating character, the electronic and magnetic structures were not consistent with experimental data; for example, the band gap was estimated to be about 10 eV. Franchini *et al.* employed density functional theory (DFT) with Perdew-Burke-Ernzerhof (PBE), PBE plus U_{eff} (PBE+U_{eff}), and hybrid functionals to investigate the ground-state properties of Mn_3O_4 [17]. The ground state was found to be half metal with ferrimagnetic ordering using the PBE+U_{eff} functional, whereas a ferrimagnetic insulator ground state was obtained within the hybrid functional. The findings also revealed that PBE+U_{eff} favors a half-metallic state in oxygen-rich Mn oxides, such as Mn_3O_4, Mn_2O_3, and MnO_2. Riberio *et al.* further compared the ground states of Mn_3O_4 obtained using different hybrid functionals [18]. Recently, Lim *et al.* reported that DFT+U+J reproduced a YK-FiM insulator with a band gap of 1 eV as a ground state [19]. They found that the DFT+U+J calculation with an explicit exchange correction for the intraorbital Coulomb potential can accurately describe the ground state of Mn oxides containing Mn^{3+} or Mn^{4+}. Reliable first-principles calculations at the DFT+U level are of

*Present address: Materials Science and Technology Division, Oak Ridge National Laboratory, Oak Ridge, Tennessee 37831, USA.
†Corresponding author: mkim@snu.ac.kr
‡Corresponding author: ykkwon@khu.ac.kr

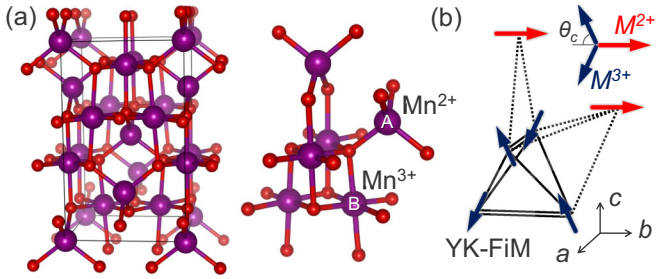

FIG. 1. (a) Crystal structure of the tetragonal Mn_3O_4 (left) and its local coordination with Mn^{2+} occupying the tetrahedral A site and Mn^{3+} occupying the octahedral B site (right). The purple and red balls denote Mn and O atoms, respectively. (b) Schematic of noncollinear spin configuration in the low-temperature Yafet-Kittel ferrimagnetic (YK-FiM) phase of Mn_3O_4 corresponding to the right structure in (a). The red and black arrows indicate the spins of the Mn^{2+} and Mn^{3+} atoms, respectively. The detailed magnetic structure of the YK-FiM phase is explained in the main text.

particular value because their low computational costs enable a variety of large-scale supercell calculations.

In this study, we systematically investigated the effects of anisotropic Coulomb interactions on the electronic and magnetic properties of Mn_3O_4 within the framework of DFT+U+J calculations. We found that the anisotropic interaction in Mn^{3+} causes significant variations in various physical properties including the band gap, local magnetic moments, canted angle, spontaneous magnetic moment, and exchange coupling constants. Meanwhile, the anisotropic interaction in Mn^{2+} was fully compensated without any noticeable effects. We found that the spin transfer into the Mn^{3+} $d_{x^2-y^2}$ orbital is primarily tuned by the anisotropic interaction, triggering modification of the 90° correlation superexchange and noncollinear magnetic structure. These findings demonstrate why the anisotropic Coulomb correction is required in DFT+U calculations for various Mn oxides.

II. METHODOLOGY AND COMPUTATIONAL DETAILS

DFT sometimes fails to describe the electronic structure of transition metal oxides with partially filled d orbitals, due to the spurious self-interaction error that causes the localized d state to be improperly destabilized [20,21]. This error can be effectively corrected by employing Hubbard-U type corrections for the localized orbitals, known as DFT+U. Two correction schemes have been used for the DFT+U approach, i.e., the spherically averaged scheme suggested by Dudarev [22] (DFT+U_{eff}) and the rotationally invariant scheme proposed by Lichtenstein [23] (DFT+U+J). In the DFT+U_{eff}, the Coulomb interactions in the same d orbital (direct Coulomb interactions) are corrected by a single U_{eff} parameter, and the interactions between the different d orbitals (anisotropic Coulomb interactions) are set to be identical to the averaged value. In contrast, the direct and anisotropic Coulomb interactions are corrected separately by the Hubbard U and exchange J in the DFT+U+J. Nearly no significant differences were observed for most materials regardless of which scheme was used. However, it has recently been shown that the anisotropic Coulomb interaction makes a critical difference in some multiorbital systems, including Mn oxides with Mn^{3+} or Mn^{4+}, such as Mn_3O_4 [19], Mn_2O_3 [19], MnO_2 [19,24,25], and $LaMnO_3$ [26].

In the DFT+U+J methodology, the DFT total energy is complemented not only by the direct and anisotropic Coulomb interactions, but also by considering the double-counted exchange energy correction, and is thus given by [26]

$$E_{\text{DFT}+U+J} = E_{\text{DFT}} + \frac{(U-J)}{2}\sum_{i,\sigma}{}' f_{i\sigma}(1-f_{i\sigma}) + \frac{1}{2}\sum_{\substack{i,\sigma\\ j,\sigma'}}{}' \left(C_{ij}^{\sigma\sigma'} f_{i\sigma} f_{j\sigma'} - \Delta X_{ij}^{\sigma} f_{i\sigma} f_{j\sigma'} \delta_{\sigma\sigma'}\right), \tag{1}$$

where $\sum'$ indicates summation over only the Hubbard-U corrected atoms, and $f_{i\sigma}$ is the eigenoccupation of the on-site density matrix with orbital and spin indices i and σ. In this equation, the first term E_{DFT} is the total energy computed with electron-density based exchange-correlation functionals (PBE in this study), and the second term is the isotropic Coulomb correction part, the coefficient $(U-J)$ of which is identical to the effective Hubbard parameter U_{eff} used in the DFT+U_{eff} or Dudarev scheme [22]. The third term is the anisotropic Coulomb correction part, in which two coefficients $C_{ij}^{\sigma\sigma'}$ and ΔX_{ij}^{σ} are the specialized Coulomb and double-counting corrected exchange matrix elements for anisotropic interorbital interactions, respectively, as defined by Mellan *et al.* [26]. Note that for isotropic cases, these matrices average to zero, being reduced to the DFT+U_{eff} scheme. In contrast, for anisotropic cases, these correction matrices are regarded as additional Coulombic and exchange corrections induced from the angular characters of interactions. Thus, the $U+J$ correction $\Delta\epsilon_{i\sigma}$ to the DFT energy eigenvalue $\epsilon_{i\sigma}^{\text{DFT}}$ can be evaluated by taking the derivative of the correction parts in Eq. (1) with respect to $f_{i\sigma}$ as

$$\begin{aligned}\Delta\epsilon_{i\sigma} &= \frac{\partial(E_{\text{DFT}+U+J} - E_{\text{DFT}})}{\partial f_{i\sigma}} \\ &= (U-J)\left(\frac{1}{2} - f_{i\sigma}\right) + \sum_{j\sigma'}\left(C_{ij}^{\sigma\sigma'} f_{j\sigma'} - \Delta X_{ij}^{\sigma} f_{j\sigma'}\delta_{\sigma\sigma'}\right).\end{aligned} \tag{2}$$

Equation (2) can be expressed in a more compact vector-matrix multiplication, especially for anisotropic d orbital systems, the correction matrices $C^{\sigma\sigma'}$ and ΔX^{σ} of which are proportional to the exchange parameter J, as [26]

$$\Delta\epsilon_{\sigma} = (U-J)\left(\tfrac{1}{2} - f_{\sigma}\right) + J(A^{\sigma} f_{\sigma} + B^{\sigma} f_{\bar{\sigma}}), \tag{3}$$

where $\bar{\sigma}$ denotes the opposite spin to σ, and $A^{\sigma} = (C^{\sigma\sigma} - \Delta X^{\sigma})/J$ and $B^{\sigma} = C^{\sigma\bar{\sigma}}/J$ are dimensionless matrices. In

terms of a basis set composed of the e_g ($d_{x^2-y^2}$ and $d_{3z^2-r^2}$) and t_{2g} (d_{xy}, d_{yz}, and d_{zx}) orbitals, the matrix elements of these dimensionless matrices can be evaluated as [26]

$$A^{\sigma} = \begin{pmatrix} 0.00 & -0.52 & 0.86 & -0.17 & -0.17 \\ -0.52 & 0.00 & -0.52 & 0.52 & 0.52 \\ 0.86 & -0.52 & 0.00 & -0.17 & -0.17 \\ -0.17 & 0.52 & -0.17 & 0.00 & -0.17 \\ -0.17 & 0.52 & -0.17 & -0.17 & 0.00 \end{pmatrix}$$

and

$$B^{\sigma} = \begin{pmatrix} 1.14 & -0.63 & 0.29 & -0.40 & -0.40 \\ -0.63 & 1.14 & -0.63 & 0.06 & 0.06 \\ 0.29 & -0.63 & 1.14 & -0.40 & -0.40 \\ -0.40 & 0.06 & -0.40 & 1.14 & -0.40 \\ -0.40 & 0.06 & -0.40 & -0.40 & 1.14 \end{pmatrix}.$$

DFT+U+J calculations were carried out using the Vienna *ab initio* simulation package (VASP) code [27]. We used the PBE functional [28] for the exchange-correlation functional, and the projected-augmented-wave (PAW) method [29] was applied to describe the potential of the core electrons. We defined the U and J parameters separately for Mn^{2+} and Mn^{3+} to investigate the role of anisotropic interactions at each site. The energy cutoff for the plane-wave basis set was 500 eV and a Γ-centered 6×6×4 Monkhorst-Pack grid was used for sampling the Brillouin zone. In this study, we fixed the lattice parameters to the experimental values for all calculations, i.e., $a = b = 5.76$ Å and $c = 9.46$ Å [33]. We considered only the experimental YK-FiM phase, which is the ground state of Mn_3O_4 also verified in the DFT+U+J scheme [19].

III. RESULTS

The exchange parameter J plays two different roles in the Hubbard correction of the band energy eigenvalues as shown in Eq. (3). On the one hand, the strength of the direct Coulomb repulsion is reduced by J as in $(U - J)$, which is the same as U_{eff} in the Dudarev scheme [22]. On the other hand, J contributes an additional orbital splitting as a direct consequence of the interorbital interactions. By comparing the numerical results computed with different J while keeping $(U - J)$ constant, we can focus solely on the role of anisotropic interactions in the electronic and magnetic properties of Mn_3O_4. That is, we scanned the Hubbard-U parameter space with the axes $(U - J)^{2+}$, $(U - J)^{3+}$, J^{2+}, and J^{3+}, not the axes U^{2+}, U^{3+}, J^{2+}, and J^{3+}.

A. Electronic structures

For typical parameter values of $(U - J)^{2+} = 4$ eV and $(U - J)^{3+} = 2$ eV, we first calculated densities of states (DOSs) of Mn_3O_4 with different values of the J^{2+} and J^{3+} parameters. The results revealed that the anisotropic Coulomb interaction in Mn^{3+} played a more significant role in orbital energies than that in Mn^{2+}, increasing the band gap from 1.3 eV with $J^{3+} = 0$ eV to 1.6 eV with $J^{3+} = 1.5$ eV, as shown in Fig. 2(a). This finding suggests that the anisotropic interaction in Mn^{3+} would have greater effects on superexchange coupling in Mn_3O_4. In contrast, the anisotropic interactions in Mn^{2+} did not cause any change in the orbital energies. The insensitivity of Mn^{2+} is attributed

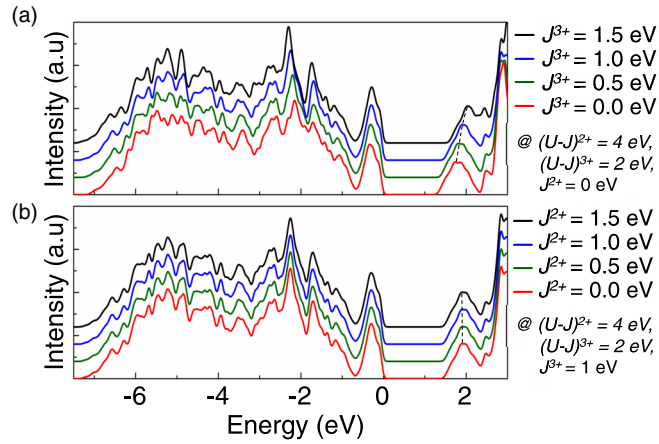

FIG. 2. Densities of states (DOSs) of YK-FiM Mn_3O_4 calculated for fixed values of $(U - J)^{2+} = 4$ eV and $(U - J)^{3+} = 2$ eV (a) with varying J^{3+} values and a fixed value of $J^{2+} = 0$ eV, and (b) with varying J^{2+} and a fixed value of $J^{3+} = 1$ eV. The dashed lines indicate trends of change in the conduction band edge due to the anisotropic Coulomb interactions J^{3+} and J^{2+}.

to their orbital occupations. The Mn^{2+} in Mn_3O_4 have a high-spin d_5 orbital occupation with majority-spin orbitals fully occupied while the minority-spin orbitals are completely empty. In this electron configuration, the anisotropic Coulomb interactions are fully compensated, and the orbital energies are unaffected by the anisotropic interactions. This result further verifies why the anisotropic Coulomb interactions are particularly important for manganese oxides with Mn^{3+} or Mn^{4+} but not for MnO [17,30–32].

B. Magnetic properties

Several magnetic observables of the YK-FiM Mn_3O_4 were evaluated while adjusting the Hubbard parameters. These observables were represented in a color-coded contour map with $(U - J)^{2+}$ and $(U - J)^{3+}$ as the x and y axes while changing J^{3+} values from 0.0 eV to 1.5 eV. For a given specific J^{3+} value, each was displayed in color-coded contour maps as a different function set. Figures 3(a) and 3(b) present the local magnetic moments of M^{2+} and M^{3+}, respectively. The finding revealed that the former increases as $(U - J)^{2+}$ increases, while the latter increases as $(U - J)^{3+}$ increases. This is consistent with previous observations that the direct Coulomb repulsion enhances the spin and orbital polarizations. Moreover, while M^{2+} appears to be relatively independent of the exchange J^{3+} value, M^{3+} tends to decrease as the exchange J^{3+} increases, as displayed in Figs. 3(a) and 3(b). These observations indicate that the anisotropic interaction in Mn^{3+} reduces its local magnetic moments. Additionally, the canted angle and the spontaneous magnetic moment are also modified by the anisotropic interaction in Mn^{3+}, as shown in Figs. 3(c) and 3(d). Both the canted angle and the spontaneous magnetic moment decrease monotonically as the exchange J^{3+} increases. Our results confirm that the anisotropic Coulomb interactions in Mn^{3+} are the crucial factors in determining the magnetic ground state of Mn_3O_4.

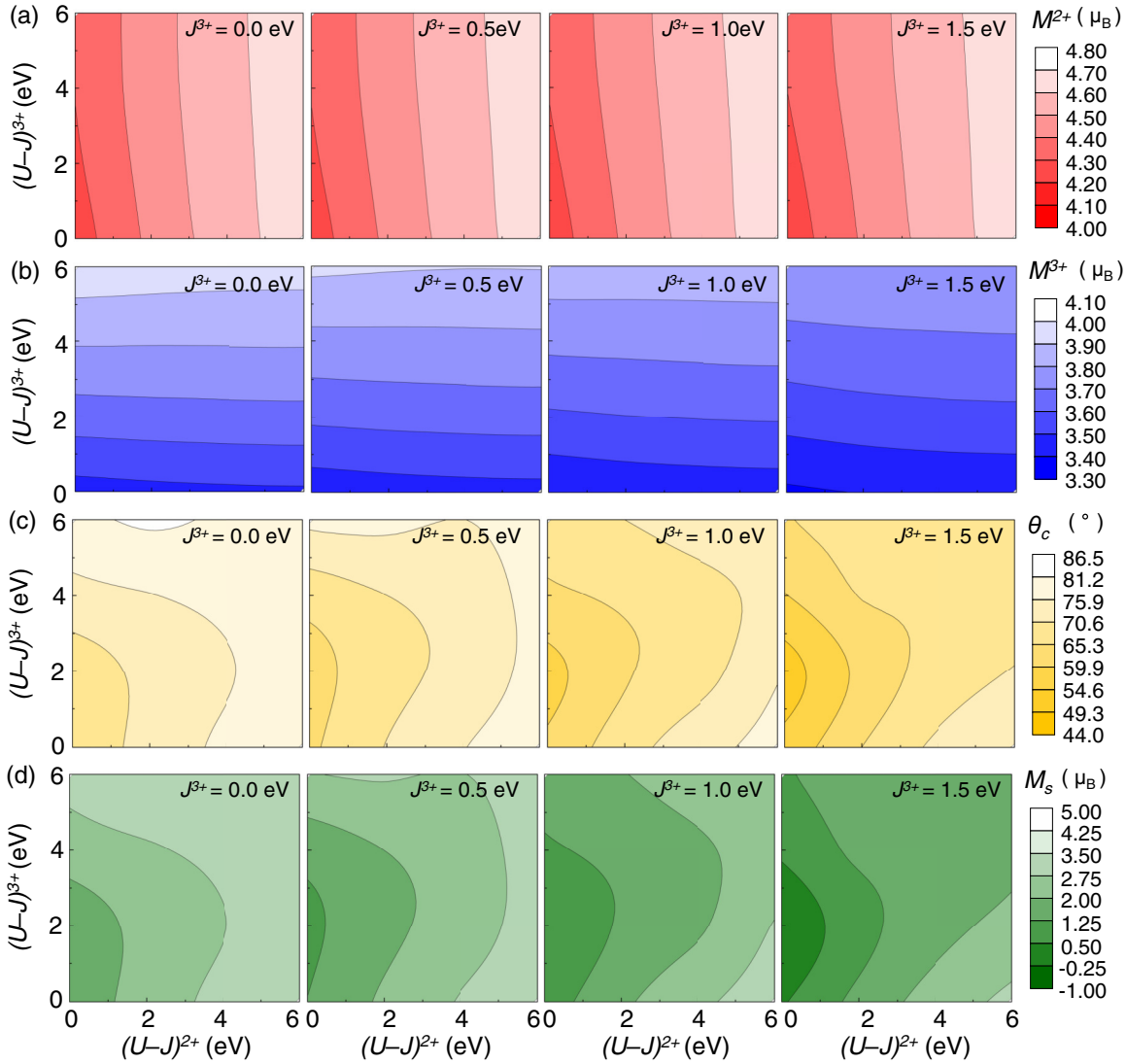

FIG. 3. Contour maps for local magnetic moments (a) M^{2+} and (b) M^{3+}, respectively, of Mn^{2+} and Mn^{3+}, (c) canted angle θ_c defined in Fig. 1 (b), and (d) spontaneous magnetic moments M_s of YK-FiM Mn_3O_4 evaluated with different sets of Hubbard parameters. Each map presents its corresponding magnetic property as a function of the effective Hubbard parameters $(U-J)^{2+}$ and $(U-J)^{3+}$ at a specific J^{3+} with $J^{2+}=0$ eV. The contour maps for each quantity are color-coded according to the values given in the scale bar.

We further explored the effects of J^{3+} on three different interatomic exchange couplings of Mn_3O_4 classified as follows. As shown in Fig. 4(a), J_{BB1} indicates the short-distance interaction between two neighboring octahedral B-site ions located within the same chain along either the a or b direction, whereas J_{BB2} represents the long-distance interchain interaction between two perpendicular octahedral chains. J_{AB} denotes the exchange coupling constant between neighboring tetrahedral A- and octahedral B-site ions. The exchange coupling constants were extracted by mapping the energies of various magnetic disorders onto a classical Heisenberg Hamiltonian

$$H = J_{BB1}\sum_{BB1}\mathbf{S}_i\cdot\mathbf{S}_j + J_{BB2}\sum_{BB2}\mathbf{S}_i\cdot\mathbf{S}_j + J_{AB}\sum_{AB}\mathbf{S}_i\cdot\mathbf{S}_j,$$

where $\mathbf{S}_i\cdot\mathbf{S}_j$ is the inner product between two spins localized at i and j sites [31]. Each summation is allowed only over the pairs of spins constrained by its corresponding subscript. In this Hamiltonian, we did not consider the superexchange interaction J_{AA} between two neighboring tetrahedral A-site ions because it is expected to be significantly weaker than other superexchange couplings. J_{AA} involves two oxygen bridges, while the other superexchange interactions J_{BB1}, J_{BB2}, and J_{AB} involve only one bridge, as shown in Fig. 1(a). These three fitted exchange coupling constants are presented as a function of J^{3+} with constant values of $(U-J)^{2+}=4$ eV, $(U-J)^{3+}=2$ eV, and $J^{2+}=0$ eV in Fig. 4(b). J_{BB1}, which is always positive indicating the antiferromagnetic (AFM) intrachain interaction, is notably attenuated by the anisotropic interaction, while the interchain exchange coupling J_{BB2} induces the transformation from the AFM to ferromagnetic (FM) state with the anisotropic interaction J^{3+} as indicated by its sign change. In contrast, J_{AB} becomes stronger with increasing strength of the anisotropic interaction, maintaining the AFM interaction between A- and B-site ions. The strong AFM J_{BB1} and the weak FM J_{BB2} are the key features of

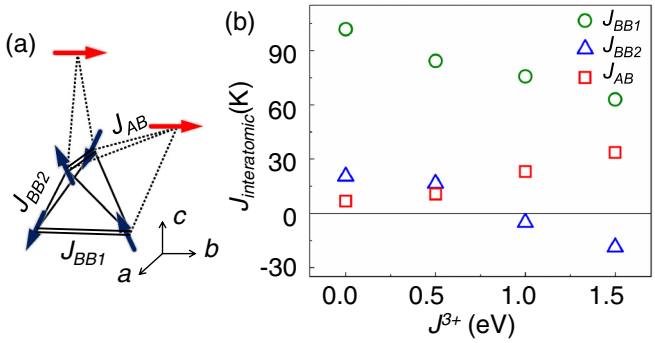

FIG. 4. (a) Different interatomic exchange couplings J_{BB1}, J_{BB2}, and J_{AB} marked in the schematic spin configuration of the YK-FiM Mn_3O_4 shown in Fig. 1(b). J_{BB1} indicates the short-distance interaction between two neighboring octahedral B-site ions within the same chain along either the a or b direction, whereas J_{BB2} represents the long-distance interchain interaction between two perpendicular octahedral chains. J_{AB} denotes the exchange coupling constant between neighboring tetrahedral A- and octahedral B-site ions. (b) Three exchange coupling constants J_{BB1}, J_{BB2}, and J_{AB} as a function of the exchange parameter J^{3+} verifying their dependence on the anisotropic Coulomb interactions of Mn^{3+}.

magnetic interactions in Mn_3O_4, measured by inelastic neutron scattering experiments [12]. Our results demonstrate that this key characteristic is determined by the anisotropic Coulomb interactions in Mn^{3+}.

C. Optimal parameters of Hubbard U and exchange J for Mn_3O_4

With $(U-J)^{2+}=4$ eV, $(U-J)^{3+}=2$ eV, $J^{2+}=0$ eV, and $J^{3+}=1$ eV, we applied the DFT+U+J scheme to evaluate various magnetic properties, such as local magnetic moments (M^{2+} and M^{3+}), spontaneous magnetic moment ($M^{\rm spon}$), canted angle ($\theta^{\rm cant}$), and exchange coupling constants (J_{BB1}, J_{BB2}, and J_{AB}). As summarized in Table I together with the corresponding experimental data [6,12], our DFT+U+J calculations accurately reproduced its magnetic moments and canted angle observed experimentally. Importantly, the weak FM interchain superexchange was also predicted by this set of Hubbard parameters. The optimal Hubbard parameters were different for Mn^{2+} and Mn^{3+}, suggesting that the effective Coulomb interaction that acts on d electrons may vary depending on the oxidation states, local symmetry, and/or hybridization. Specifically, the direct Coulomb interaction in Mn^{2+} [$(U-J)^{2+}=4$ eV] is stronger than that in Mn^{3+} [$(U-J)^{3+}=2$ eV]. The reduced Coulomb interaction in Mn^{3+} can be attributed to its strong charge-transfer or hybridization character [34]. In this study, we considered separate Hubbard parameters for Mn^{2+} and Mn^{3+} to clarify the role of each on-site interaction in the electronic and magnetic properties of Mn_3O_4. It may be difficult to define the Hubbard parameters separately when investigating the physical properties of nonbulk configurations such as surfaces, interfaces, and defects. In this case, $U=4.0$ eV and $J=1.2$ eV, as employed by Lim *et al.*, would be a reasonable choice for a single set of Hubbard parameters for Mn_3O_4 [19]. However, the weak FM interchain interactions are not reproduced in calculations using a single set of Hubbard parameters, although the overall results are qualitatively consistent with our results [19]. It is worth noting that changing U and J parameters would influence the Jahn-Teller effects resulting in the structural modification, which again affects the roles of U and J, and so on. Such an interplay between structural distortion and anisotropic Coulomb interactions may provide subtle effects on various properties of Mn_3O_4. However, we were not able to systematically examine their interplay in this study since it requires a complete scan over the whole U and J parameter space by finding the fully optimized structure at every set of U and J parameters or a self-consistent optimization of the U and J parameters and the geometric parameters, either one of which is indeed beyond the our computational capability.

IV. DISCUSSION

The eigenoccupations of the on-site d orbital density matrix (f_σ) are fictitious auxiliary physical quantities, but they can often provide a direct insight into the orbital states of the transition metal ions [25,26]. With $(U-J)^{2+}=4$ eV, $(U-J)^{3+}=2$ eV, $J^{2+}=0$ eV, and $J^{3+}=0$ eV, the eigenoccupations of the A- and B-site Mn atoms were calculated to be

$$(f_\sigma|f_{\bar\sigma}) = \begin{pmatrix} 0.940 & 0.018 \\ 0.943 & 0.025 \\ 0.944 & 0.062 \\ 0.948 & 0.059 \\ 0.944 & 0.061 \end{pmatrix} \quad \text{and}$$

$$(f_\sigma|f_{\bar\sigma}) = \begin{pmatrix} 0.456 & 0.287 \\ 0.960 & 0.142 \\ 0.943 & 0.067 \\ 0.951 & 0.082 \\ 0.939 & 0.057 \end{pmatrix},$$

TABLE I. Various magnetic properties of the Yafet-Kittel phase of Mn_3O_4 evaluated with $(U^{2+},J^{2+})=(4,0)$ eV and $(U^{3+},J^{3+})=(3,1)$ eV. The corresponding experimental values are given for comparison [4–6,12,33].

M^{2+} (μ_B)	M^{3+} (μ_B)	$M^{\rm spon}$ (μ_B)	$\theta^{\rm cant}$ (deg)	J_{BB1} (K)	J_{BB2} (K)	J_{AB} (K)	
4.56	3.61	1.77	67.6	75.7	−5.2	23.08	This work
4.57	3.51	1.89	66.9				Ref. [6]
				55.1	−3.2	6.3	Ref. [12]
		1.84					Ref. [5]
4.65	3.55	1.85	69.3				Ref. [33]
				19.9	19.9	6.8	Ref. [4]

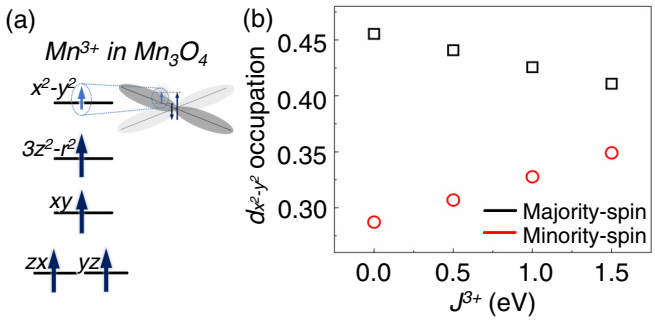

FIG. 5. (a) Schematic of the d orbital levels and the orbital occupations of an Mn^{3+} ion in Mn_3O_4. The inset explains the partially occupied $d_{x^2-y^2}$ orbital, which is attributed to the spin transfer from O^{2-}. The spin transfer through this unoccupied channel determines the correlation superexchange of Mn_3O_4. (b) $d_{x^2-y^2}$ orbital occupations of the majority and minority spins of the Mn^{3+} ion as a function of the exchange parameter J^{3+}.

respectively, where the occupations of the $d_{x^2-y^2}$, $d_{3z^2-r^2}$, d_{xy}, d_{yz}, and d_{zx} orbitals are presented from top to bottom. The A-site Mn^{2+} ion was confirmed to have a high-spin (HS) d_5 orbital configuration (HS Mn^{2+}) with all majority-spin orbitals almost fully occupied but minority-spin orbitals nearly empty. The result for the Mn^{3+} ion, on the other hand, shows that the four lower energy d orbitals are fully occupied for majority-spin $d_{3z^2-r^2}$, d_{xy}, d_{yz}, and d_{zx} orbitals, which is consistent with the HS Mn^{3+} configuration. Interestingly, the majority- and minority-spin $d_{x^2-y^2}$ orbitals, which are expected to be fully empty in the ideal Mn^{3+} configuration, were partially occupied in Mn_3O_4, which is attributed to the charge transfer from O^{2-}, as depicted in Fig. 5(a). Furthermore, the level of occupation of the majority-spin $d_{x^2-y^2}$ orbitals is different from that of the minority-spin $d_{x^2-y^2}$ orbitals, resulting in a net spin moment in the $d_{x^2-y^2}$ orbital. The spin transfer into this orbital is a key element in determining the correlative superexchange of Mn_3O_4.

We first explored how the orbital occupation of Mn^{3+} varies with the strength of its anisotropic interaction. The occupations of the four lower occupied orbitals rarely depend on the anisotropic Coulomb interaction, whereas that of the $d_{x^2-y^2}$ orbital is systematically modified, as shown in Fig. 5(b). Its minority- and majority-spin orbitals become more and less occupied with the anisotropic interactions, respectively, resulting in the reduction of the net spin moment, which can be interpreted as the spin transfer into the $d_{x^2-y^2}$ orbital channel, but its total occupation remains. The reduced net spin moment is consistent with the reduction in the local magnetic moments M^{3+} of Mn^{3+} shown in Fig. 3(b).

The magnetic interaction between two neighboring Mn^{3+} ions, which are connected via an O^{2+} ion to each other at 90°, is governed by two different exchange couplings [12,35]. One is the direct overlap between d_{xy} orbitals, causing the short-distance intrachain interaction J_{BB1} to be very strongly AFM, while the second is the 90° correlation superexchange referring to the magnetic interaction whereby two electrons of an O^{2-} ion relay the exchange coupling between neighboring cations [35]. Importantly, the strongest spin channel for the correlation superexchange always involves the $d_{x^2-y^2}$ orbitals, and the anisotropic Coulomb interaction determines this spin channel. The anisotropic interaction reduces the AFM interaction in J_{BB1} due to the weakened correlation superexchange by a shrunken spin channel. The sign of the 90° correlation superexchange is very sensitive to the characteristics of the broker electrons in the O^{2-} ions [35]. If two electrons relaying the 90° correlation superexchange are from the same orbital, the magnetic interaction remains AFM keeping the sign; however, if they are from different (and orthogonal) orbitals, the interaction may become FM through the sign change. That is, the orbital and hybridization states of O^{2-} determine the sign of the 90° correlation superexchange. The reduced net spin transfer may have perturbed the hybridized state of the O^{2-} ions, yielding the transition of J_{BB2} from weak AFM to weak FM.

V. CONCLUSION

We analyzed the role of the anisotropic Coulomb interaction in the electronic and magnetic ground state of mixed-valent Mn_3O_4 within the framework of DFT+U+J with separate sets of distinct Hubbard parameters for Mn^{2+} and Mn^{3+}. The anisotropic interaction J^{3+} of the Mn^{3+} ion extensively affects a variety of ground-state properties such as the band gap, local magnetic moments, canted angle, spontaneous magnetic moments, and superexchange coupling, while J^{2+} the counterpart of the Mn^{2+} ion is fully compensated without any noticeable changes. The 90° correlation superexchange is characterized by the spin transfer into the $d_{x^2-y^2}$ orbital of the Mn^{3+} ion, which can be controlled by the anisotropic interaction in Mn^{3+}. The DFT+U+J calculations with the sizable anisotropic interaction J^{3+} reproduce the weak FM interchain interactions, which has not been obtained in previous calculations. The best description was achieved when $U^{2+} = 4$ eV, $J^{2+} = 0$ eV, $U^{3+} = 3$ eV, and $J^{3+} = 1$ eV. This study provides important insights into why the exchange parameter J should be explicitly taken into account in Hubbard corrections, especially exchange Mn oxides with Mn^{3+} or Mn^{4+} such as Mn_3O_4, Mn_2O_3, MnO_2, and $LaMnO_3$. The anisotropic interactions strongly modify the spin transfer into unoccupied d orbitals, leading to significant corrections of interatomic superexchange interactions.

ACKNOWLEDGMENTS

We gratefully acknowledge financial support from the Korean government (MSIT) through the National Research Foundation (NRF) of Korea (Grants No. 2019R1A2C1005417, No. 2017M3D1A1040688, and No. 2017R1A2B3011629). A portion of our computational work was done using the resources of the KISTI Supercomputing Center (KSC-2020-CRE-0011).

[1] M. Kim, X. M. Chen, Y. I. Joe, E. Fradkin, P. Abbamonte, and S. L. Cooper, Phys. Rev. Lett. **104**, 136402 (2010).
[2] S. L. Gleason, T. Byrum, Y. Gim, A. Thaler, P. Abbamonte, G. J. MacDougall, L. W. Martin, H. D. Zhou, and S. L. Cooper, Phys. Rev. B **89**, 134402 (2014).
[3] Y. Nii, H. Sagayama, H. Umetsu, N. Abe, K. Taniguchi, and T. Arima, Phys. Rev. B **87**, 195115 (2013).
[4] G. Srinivasan and M. S. Seehra, Phys. Rev. B **28**, 1 (1983).
[5] K. Dwight and N. Menyuk, Phys. Rev. **119**, 1470 (1960).
[6] B. Chardon and F. Vigneron, J. Magn. Magn. Mater. **58**, 128 (1986).
[7] R. Tackett, G. Lawes, B. C. Melot, M. Grossman, E. S. Toberer, and R. Seshadri, Phys. Rev. B **76**, 024409 (2007).
[8] T. Suzuki and T. Katsufuji, Phys. Rev. B **77**, 220402(R) (2008).
[9] M. C. Kemei, J. K. Harada, R. Seshadri, and M. R. Suchomel, Phys. Rev. B **90**, 064418 (2014).
[10] S. Pal and S. Lal, Phys. Rev. B **96**, 075139 (2017).
[11] S. Thota, F. Guillou, V. Hardy, A. Wahl, W. Prellier, and J. Kumar, J. Appl. Phys. **109**, 053902 (2011).
[12] J.-H. Chung, J.-H. Kim, S.-H. Lee, T. J. Sato, T. Suzuki, M. Katsumura, and T. Katsufuji, Phys. Rev. B **77**, 054412 (2008).
[13] S. Hirai, Y. Goto, Y. Sakai, A. Wakatsuki, Y. Kamihara, and M. Matoba, J. Phys. Soc. Jpn. **84**, 114702 (2015).
[14] D. Dubal, D. Dhawale, R. Salunkhe, V. Fulari, and C. Lokhande, J. Alloys Compd. **497**, 166 (2010).
[15] A. Jha, R. Thapa, and K. Chattopadhyay, Mater. Res. Bull. **47**, 813 (2012).
[16] A. Chartier, P. D'Arco, R. Dovesi, and V. R. Saunders, Phys. Rev. B **60**, 14042 (1999).
[17] C. Franchini, R. Podloucky, J. Paier, M. Marsman, and G. Kresse, Phys. Rev. B **75**, 195128 (2007).
[18] R. Ribeiro, S. de Lazaro, and S. Pianaro, J. Magn. Magn. Mater. **391**, 166 (2015).
[19] J. S. Lim, D. Saldana-Greco, and A. M. Rappe, Phys. Rev. B **94**, 165151 (2016).
[20] M. Cococcioni and S. de Gironcoli, Phys. Rev. B **71**, 035105 (2005).
[21] N. J. Mosey, P. Liao, and E. A. Carter, J. Chem. Phys. **129**, 014103 (2008).
[22] S. L. Dudarev, G. A. Botton, S. Y. Savrasov, C. J. Humphreys, and A. P. Sutton, Phys. Rev. B **57**, 1505 (1998).
[23] A. I. Liechtenstein, V. I. Anisimov, and J. Zaanen, Phys. Rev. B **52**, R5467 (1995).
[24] E. Cockayne and L. Li, Chem. Phys. Lett. **544**, 53 (2012).
[25] D. A. Tompsett, D. S. Middlemiss, and M. S. Islam, Phys. Rev. B **86**, 205126 (2012).
[26] T. A. Mellan, F. Cora, R. Grau-Crespo, and S. Ismail-Beigi, Phys. Rev. B **92**, 085151 (2015).
[27] G. Kresse and J. Furthmüller, Phys. Rev. B **54**, 11169 (1996).
[28] J. P. Perdew, K. Burke, and M. Ernzerhof, Phys. Rev. Lett. **77**, 3865 (1996).
[29] G. Kresse and D. Joubert, Phys. Rev. B **59**, 1758 (1999).
[30] C. Franchini, V. Bayer, R. Podloucky, J. Paier, and G. Kresse, Phys. Rev. B **72**, 045132 (2005).
[31] S. Yoon, S.-H. Kang, S. Lee, K. Kim, J.-P. Song, M. Kim, and Y.-K. Kwon, Phys. Chem. Chem. Phys. **21**, 15932 (2019).
[32] S. Yoon, K. Jin, S. Lee, K. T. Nam, M. Kim, and Y.-K. Kwon, Phys. Chem. Chem. Phys. **23**, 859 (2021).
[33] B. Boucher, R. Buhl, and M. Perrin, J. Phys. Chem. Solids **32**, 2429 (1971).
[34] F. De Groot, Coord. Chem. Rev. **249**, 31 (2005).
[35] J. B. Goodenough, *Magnetism and the Chemical Bond*, Vol. 1 (Interscience Publishers, New York, 1963).